DESIGN STUDY OF LCLS CHIRP-CONTROL WITH A CORRUGATED STRUCTURE

Z. Zhang, K. Bane, Y. Ding, Z. Huang, R. Iverson, T. Maxwell, G. Stupakov, L. Wang
SLAC National Accelerator Laboratory, Menlo Park, CA 94025, USA
M. Ruelas, M. Harrison, P. Frigola
Radiabeam Systems, Santa Monica, CA 90404, USA

Abstract

The purpose of this paper is to investigate the use of flat metallic plates with small corrugations as a passive dechirper, studying its effects on beam dynamics. Similar systems have been tested in Pohang and Brookhaven at relatively low energies (100 MeV) and with relatively long bunches (>1ps) [1,2]. Four meters of such a structure are being machined by Radiabeam Systems for use in the LCLS with a high energy and femtosecond electron beam. In this paper we use a field matching program to obtain the longitudinal and transverse wakes for the purpose of the LCLS dechirper design. In addition, we fit the longitudinal wake to simple functions, so that one can obtain the wake without resorting to the field matching program. Since the transverse wakes–both dipole and quadrupole wakes–are strong, we include beam dynamics simulations to find the tolerances for injection jitter and misalignment in the LCLS.

INTRODUCTION

In a linac-based X-ray free electron laser (FEL) there is often a need for energy chirp control of the beam as the magnetic compression employed in such FELs typically leaves an undesired time-energy correlation in the bunch, which can broaden the FEL bandwidth. While the chirp can be removed by the off-crest acceleration in a following linac section, this solution can be costly or impractical, particularly for a superconducting linac-based FEL. For such cases, a dedicated structure that can intentionally generate a strong longitudinal wakefield was recently proposed to dechirp the beam. In Ref. [3], a round metallic structure with corrugated walls was suggested and analyzed as a passive dechirper. Compared to round geometry, the flat geometry of corrugated plates has the advantage of allowing the dechirper strength to be adjusted by changing the separation of the plates [4].

In both round and flat structures, the transverse wakes can be strong, with amplitude scaling as the -4th power of aperture (vs. the -2nd power for the longitudinal wake). In a flat structure, however, in addition to the usual dipole wakefield that is excited when the beam passes through the structure off axis, there is also a quadrupole wake excited, even when the structure and beam are perfectly aligned. These transverse wakes will, if not properly controlled, increase the projected transverse emittance and lead to a deterioration of FEL performance.

Similar dechirper systems have been tested in Pohang and Brookhaven at relatively low energies (100 MeV) [1,2] and a new one is being machined for use at the LCLS [5,6].

However, when this structure is used for high energy beam, such as found in the LCLS, in order to generate a significant dechirping effect, the gap between the two plates needs to be set very small (< 1 mm). And to relax the manufacture tolerance, the size of corrugations are chosen at 0.5 mm, which is comparable to the gap size. In this case, the analytical formulas of wakefields are not applicable. In this paper the longitudinal and transverse wakes of the flat corrugation structure are calculated by the field matching method [7] and a simplified fitting formula with corrugation parameters is obtained for the longitudinal wakefield. A detailed tolerance study including beam offset, alignment error and structure imperfection is also conducted for the designed device.

FIELD MATCHING AND FITTING FORMULA

Figure 1 gives a sketch of the dechirper, showing the parameters half-gap a, corrugation period p, corrugation slit t, corrugation depth h, and width w. The wakefields of the structure are characterized by these parameters.
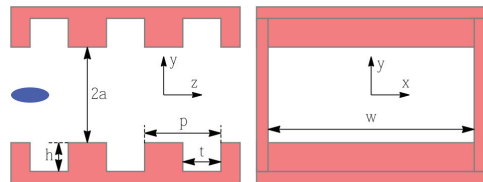

Figure 1: Geometry of dechirper structure parameters.

The analytical theory of wakefields in Ref. [3,7,8] is based on the assumption that all dimensions of the corrugations are much smaller than the gap size and the structures are deeply corrugated

$$p, h \ll a \quad \text{and} \quad h \gtrsim p \tag{1}$$

and also assuming large aspect ratio $w/2a$. The point charge wakefield for the flat pipe with small corrugations can be written as

$$W(z) = \frac{\pi^2}{16} \frac{Z_0 c}{\pi a^2} \cos(kz), \qquad z > 0 \tag{2}$$

where $Z_0 = 377\Omega$ is the characteristic impedance of vacuum and c is the speed of light. The wave number, k, is well approximated by

$$k = \sqrt{\frac{p}{aht}} \tag{3}$$

Electron Bunch Generation and Manipulation

Note that in Eq. 2, the amplitude of the wakefield is independent of the dimensions of corrugations.

However, for the LCLS dechirper, the half-gap a is very small and comparable with the corrugation size. So the analytical formulas above are not applicable in the parameter regime of interest. In order to obtain the wakefield for general case, we adopt the field matching method [7] of solving the Maxwell's Equations. The field matching program used for the numerical simulations is described elsewhere [9].

Fitting Formulas and Parameter Ranges

The form of the fitting formula for the longitudinal wakefield is assumed to be a damped cosine oscillation of the form

$$W(z) = \frac{\pi^2}{16} \frac{Z_0 c}{\pi a^2} F e^{-\frac{kz}{2Q}} \cos(kz), \quad z > 0 \qquad (4)$$

where the terms before F on the right side are the analytical amplitude of the flat metallic structure and F is the amplitude factor; k and Q are the wave number and quality factor, respectively. The three parameters are all functions of h, p, a, which will be shown in detail in the following subsections.
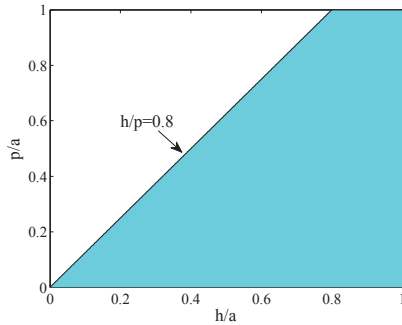

Figure 2: Validity range (colored) of the fitting formula of longitudinal wakefield.

The fitting formula Eq. 4 is valid in a specific range of interest shown in Fig. 2. We assume the dimensions of corrugations are not larger than the gap size

$$p, h \leq a \qquad (5)$$

and the corrugation is "deeply corrugated" to have a strong dominant mode

$$h/p > 0.8 \qquad (6)$$

The factor 0.8 is chosen based on the results of numerical calculation. The applications of this structure focus on the short-range wakefields, so the longitudinal range of the fitting formulas is limited to

$$kz \leq 3\pi \qquad (7)$$

We also keep $t = p/2$ for simplicity.

Fitting Results

The field matching results for F, k and Q are shown in Figs. 3, 4 and 5. Each line in Fig. 3 corresponds to a value of p/a from 0.1 to 1 and h/a is determined by the valid range requirement. The double-arrow line in Figs. 4 and 5 signify that for a given h/a, we plot all wave numbers under different p/a values ranging from 0.1 to 1. Based on these results, we can obtain the fitting formulas for these three parameters. We found that k and Q have little dependence on p/a. Actually in the analytical theory, the wave number is dependent on t/p. But we keep $t/p = 1/2$, as a constant, in the field matching calculations. The fitting forms for these three parameters of Eq. 4 are given in the following equations.

$$F(\frac{h}{a}, \frac{p}{a}) = b_1(1 - \frac{p}{a})(1 - \frac{h}{a}) + b_2(1 - \frac{h}{a}) + b_3(1 - \frac{p}{a})^2$$
$$+ b_4(1 - \frac{p}{a}) + b_5 \qquad (8)$$

$$k = \frac{1}{a}\left(\frac{c_1}{\sqrt{h/a}} + c_2\right) \qquad (9)$$

$$Q\left(\frac{h}{a}\right) = d_1\left(\frac{h}{a}\right)^2 + d_2\frac{h}{a} + d_3 \qquad (10)$$

where $b_i(i = 1, .., 5)$, c_1, c_2, d_1, d_2, d_3 are the fitting coefficients. The best fit result for these coefficients are given in Tab. 1.

Table 1: Coefficients of Best Fit for Eqs. 8,9,10 to the Field Matching Algorithm

Coefficient	Value	Coefficient	Value
b_1	0.1483	c_1	1.7096
b_2	0.1418	c_2	-0.5026
b_3	-0.0437	d_1	3.2495
b_4	0.1460	d_2	-9.1830
b_5	0.5908	d_3	10.2230

The results of the fitting formulas are also indicated in the corresponding figures by red dashed lines. It can be seen that for the amplitude factor F and wave number k the fitting formulas agree well with the results of the field matching program. The sum of the five coefficients $\sum_{i=1}^{5} b_i \approx 1$ indicates that the new formula is consistent with the analytical formula as $p/a \ll 1, h/a \ll 1$. For the quality factor Q, the precision is also good enough for applications which focus on the short-range wakefields, such as energy chirp control.

Example Longitudinal Wakefields

In this subsection, we sample some values of p, h to compare wakefields of the fitting formulas and of field matching calculations. The results are presented in Fig. 6 with the specific values of p, h written in each figure.

The wakefields are normalized by $W(0^+)$ of the analytical wakefield. It can be seen that the fitting formula Eq. 4
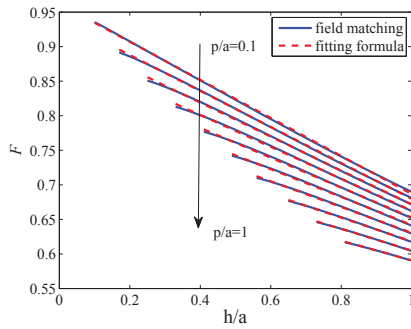
Figure 3: Amplitude factor F from field matching solution (blue solid line) and corresponding best fit to Eq. 8 (red dashed line).
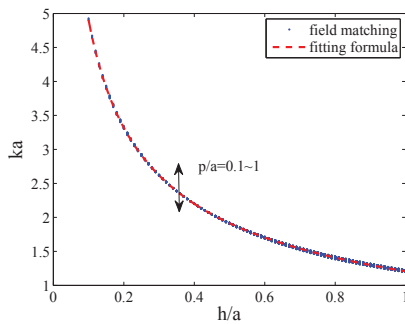

Figure 4: Wave number by field matching algorithm (blue dots) and corresponding best fit to Eq. 9 (red dashed line).
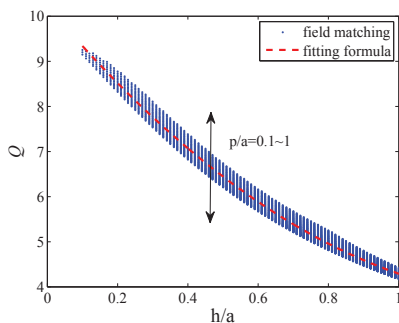

Figure 5: Quality factor by field matching algorithm (blue dots) and corresponding best fit to Eq. 10 (red dashed line).

agrees well with the results of the field matching calculation at least within the longitudinal range of $kz \leq 3\pi$. There is a little deviation in the wavelength between the two wakefields, especially when p/a and h/a are close to 1. This is because the wakefield may not behave like a cosine oscillation. If we choose other fitting forms of wave number, e.g. $k_1 z + k_2 z^2$, we can get perfect fitting results including the wave number. In that case, we need to introduce more fitting coefficients throughout, complicating the formulas. However, for the parameters under consideration, the fit as described is found to yield wakefields sufficiently consistent with all field matching solutions.
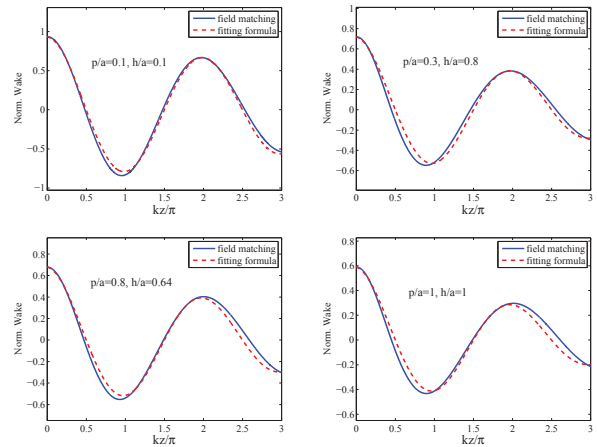
Figure 6: Examples of wakefields calculated using field matching (blue solid line) and Eq. 4 with fitting formulas Eqs. 8,9,10 (red dashed lines).

SIMULATION STUDY OF LCLS DECHIRPER

As a demonstration experiment of chirp-control for high energy beams, the dechirper will be installed at the linac-to-undulator (LTU) area of the LCLS. Essential diagnostics for the proposed dechirper experiment are shown in Fig. 7. The dechirper will be located in a low β region of the LCLS LTU. Neighboring BPMs will be used to ensure alignment through the device. A distant downstream BPM will be used to detect any deflection due to the dipole wake that may be introduced by centering errors of the dechirper. Transverse emittance measurements will be performed using LTU quads (not shown) along with the COTR-mitigated transverse profile monitor [10] at the end of LTU or, alternatively, LTU wire scanners (not shown). Finally, slice energy spread measurements will be performed in the LCLS electron dump using an X-band transverse deflecting cavity (XTCAV) [12] in conjunction with the final spectrometer bend.

The beam energy is ∼ 6.6 GeV, which will generate soft x-ray photons of 2 keV energy. The peak current after compression is ∼ 1.5 kA and the energy chirp induced by the RF off-crest acceleration is not canceled fully by the wakefield of the downstream linac. The relevant parameters of the beam are given in Tab.2.

Table 2: Beam Parameters for Proposed Dechirper Experiment

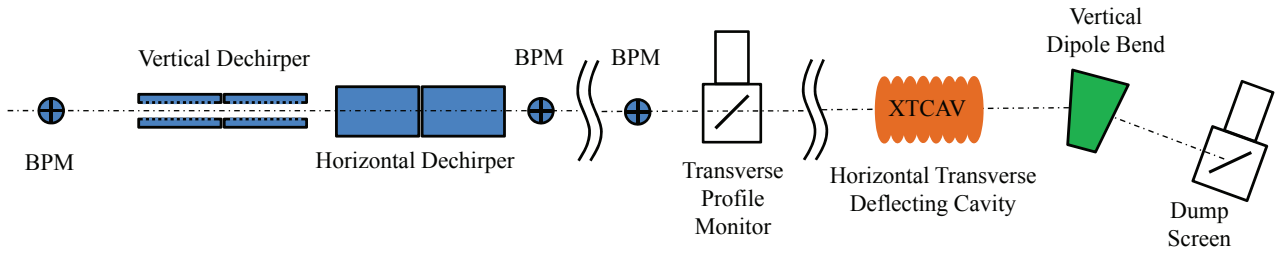| Parameter	Value	Units
Charge Q	150	pC
Peak current I_p	∼1.5	kA
Energy E	6.6	GeV
Emittance ϵ_x	0.77	μm
Emittance ϵ_y	0.39	μm
β_x	5	m
β_y	19	m

Figure 7: Schematic of the proposed dechirper experiment (not to scale). See text for description.

The total length of the dechirper is 4m in the latest design. However, the following analysis for transverse wakefields is based on Elegant [11] simulations of a 2-m-long dechirper. A longer dechirper will benefit the experiment as it allows a larger gap to achieve the same integrated longitudinal wake, while the transverse wakefields decrease more quickly with gap size. The strength of the longitudinal wake varies as $1/a^2$, while that of the transverse wakes as $1/a^4$. Thus the tolerance requirements for the new 4-meter-long dechirper will be relaxed. The structure parameters of the dechirper in the simulations are given in Tab.3.

Table 3: Structure Parameters of LCLS Dechirper in the Simulation

Parameter	Value	Units
Half-gap a	0.5/0.7	mm
Period p	0.5	mm
Depth h	0.5	mm
Slit t	0.25	mm
Width w	12	mm
Total length L	2*	m

* The total length is 4 meters in the latest design.

When $a = 0.7$ mm, the longitudinal wakefield of the structure fully cancels the remaining energy chirp. The wakefield amplitude will increase by a factor of 2 if a is set to 0.5 mm, which means over-dechirping of the beam. Figure 8 presents the longitudinal, dipole and quadrupole wakefields of the dechiper obtained by the field matching program assuming $a = 0.5$mm and other parameters in Tab.3. The simulated longitudinal phase space before and after the dechirper with $a = 0.5$ mm are shown in Fig. 9.

In the experiment of the LCLS, we can use the x-band deflecting cavity (XTCAV) located at the end of the LCLS beamline to measure longitudinal phase space [12] in Fig. 9. The final simulated images at the screen OTRDMP are given in Fig. 10, corresponding to the longitudinal phase space w/ and w/o dechirper in the beamline.The expected effect of the dechirper is clearly measurable.

Quadrupole Wakefield

The choice of dechirper parameters is determined by the following considerations. A smaller dechirper gap generates
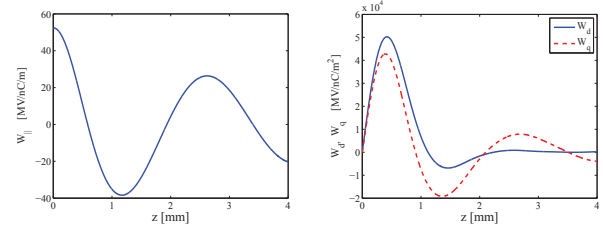

Figure 8: Longitudinal (left) and transverse (right) wake-fields of the LCLS dechirper when the gap size $a = 0.5$mm and other parameters are shown in Tab.3.
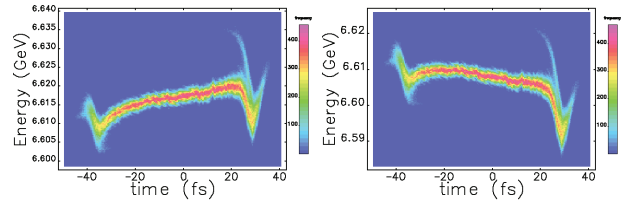

Figure 9: Longitudinal phase space before (left) and after (right) the dechirper with half-gap size $a = 0.5$mm.

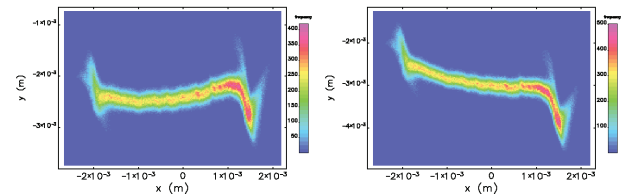Figure 10: Simulated images on the screen at OTRDMP to measure the longitudinal phase space w/o(left) and w/ (right) dechirper in the beamline.

a stronger longitudinal wakefield (which scales as $1/a^2$), and allows one to shorten the device for the required size of the energy chirp. However, an extremely small gap makes the transverse dipole and quadrupole wakefields stronger and leads to projected emittance growth and tight tolerances on the beam position jitter and dechirper alignment. Note that the transverse wakefields used in the following tolerance study are also calculated by the field matching program.

In this subsection, we consider the effect of the quadrupole wakefield, which can introduce time-dependent focusing or

defocusing on the beam to increase projected emittance. In the design, the whole dechirper will be divided into two sections of equal length. The two sections are oriented orthogonally, one with vertical plates and the other with horizontal ones. (Here the direction of dechirper is determined by the direction of the gap, e.g. the dechirper structure shown in Fig. 1 is a vertical dechirper.) Then there are four combinations for these two sections. We compare different combination types together in Fig. 11 with projected emittance increase, which is defined as

$$\frac{\delta\epsilon}{\epsilon_0} = \frac{\epsilon}{\epsilon_0} - 1 \qquad (11)$$

where ϵ_0 and ϵ are the emittance before and after the dechirper, respectively. The smaller increase in the horizontal plane is due to the smaller β value ($\beta_y = 19m, \beta_x = 5m$) and larger initial emittance before dechirper due to the CSR effect during upstream magnetic compression. It can be observed that if the two sections are oriented in the same direction, the projected emittance growth in vertical plane ($\delta\epsilon_y$) will be larger than 10% even when the beam and the device are both aligned perfectly. However, if we rotate the second section by 90° with respect to the first one, the emittance increase in both planes will become small. This verifies that the quadrupole wakefield effect can be canceled if the two sections are crossed by 90°. It is also noticed in the simulations that we need to keep similar or symmetric β values to cancel the quadrupole wakefield.

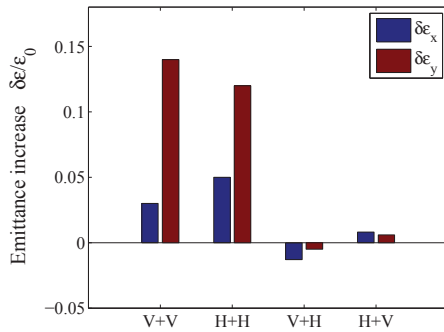Figure 11: Projected emittance increase for different combinations of the two dechirper sections."V"means vertical dechirper and "H" means horizontal dechirper.

Dipole Wakefield

If the beam enters the structure offset from the axis, it will excite the dipole wakefield. The tail of the beam will be kicked, increasing the projected emittance. In Fig. 12 we present the emittance growth versus the beam offset. Vertical (horizontal) offset leads to vertical (horizontal) emittance growth.

The asymmetric effect in the two planes is due to the different β value and ϵ_0 in the two planes. The analytical formula is derived based on Ref. [4] with the fitting formula of longitudinal wakefields Eq. 4 . It can be observed that
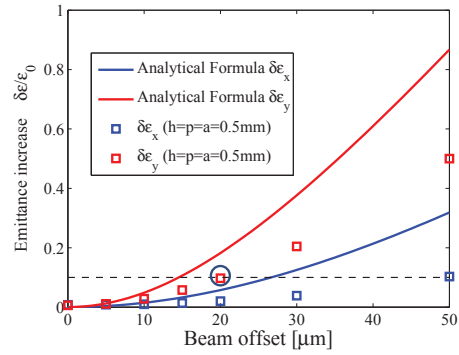

Figure 12: Projected emittance growth versus the beam offset. Vertical (horizontal) offset leads to vertical (horizontal) emittance growth.

emittance growth is more sensitive in the vertical plane and that the offset should be controlled to within $20\mu m$ if the allowed emittance growth is to be less than 10%.

Tolerance Study

In this subsection, we consider the structure tolerance of the dechirper for the experiment. We adopt the analytical methods in Ref. [4] to analyze the dipole wakefield induced by the structure error. First is the rotation error in the x direction as shown in Fig. 13. In this device, each plate has a certain angle (θ_1, θ_2) with respect to the beam path.
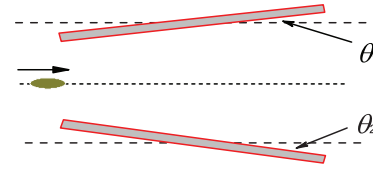

Figure 13: Dechirper with x-rotation error. Anticlockwise (clockwise) rotation corresponds to positive (negative) angle.

The emittance increase can be calculated by the method in Ref. [4] with infinitely small steps integrated along the beam path for a 1 m-long structure.

$$\left(\sqrt{\left(\frac{\epsilon}{\epsilon_0}\right)^2 - 1}\right)_{s\to s+\Delta s} = 0.375 Z_0 c \cdot \frac{\eta Q\beta\sigma_z\Delta s}{(a + s(\theta_1 - \theta_2)/2)^4 E} \cdot \frac{s(\theta_1 + \theta_2)}{2\sigma_0} \qquad (12)$$
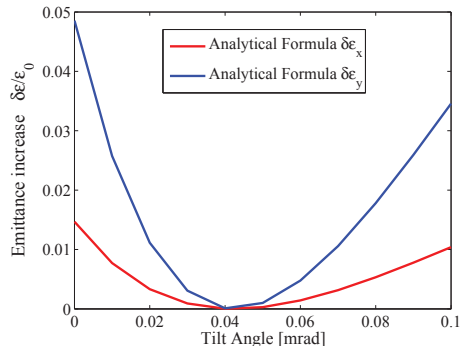
where Q is bunch charge, σ_z bunch length, σ_0 transverse beam size, E beam energy and η the amplitude factor of dipole wakefield. θ_1, θ_2 are the angles of the plates shown in Fig. 13. For simplicity, we choose θ_1 as the variable and set $\theta_2 = 0$. We plot the projected emittance increase versus the tilt angle θ_1 in Fig. 14. The dipole wake from the tilt angle leads to the increase of projected emittance and 0.1 mrad ($\theta_1 = 0.1$mrad, $\theta_2 = 0$) misalignment over 1 m length results in more than 10% emittance growth.
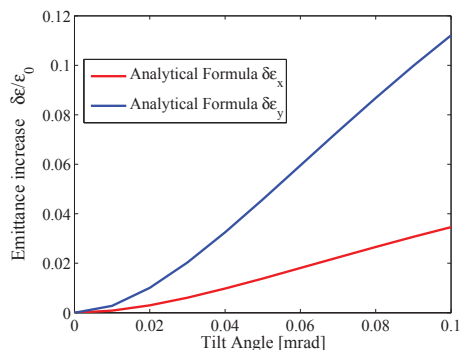
Figure 14: Emittance increase versus the tilt angle θ_1.

Figure 16: Emittance increase versus the crossing angle of two sections.

However, for a certain tilt angle we can cancel the effect of dipole wakefield by offsetting the beam at the entrance. When the beam is offset by Δ, Eq. 12 can be written as

$$\left(\sqrt{\left(\frac{\epsilon}{\epsilon_0}\right)^2 - 1}\right)_{s \to s+\Delta s} = 0.375 Z_0 c \cdot \frac{\eta Q \beta \sigma_z \Delta s}{(a + s(\theta_1 - \theta_2)/2)^4 E} \cdot \frac{s(\theta_1 + \theta_2)/2 - \Delta}{\sigma_0} \tag{13}$$

For example, if we offset beam by 10 μm, the new curve of emittance increase and the tilt angle is shown in Fig. 15. For a tilt angle, we can always find an offset value that cancels the effect of dipole wakefield.

Figure 15: Emittance increase versus the tilt angle θ_1 with offset 10μm.

Another error we consider here is the rotation angle about the longitudinal (z) axis. In the design, we cross the two sections by 90° to cancel the quadrupole wakefield. In Fig. 16, we present the emittance growth versus the crossing angle of the two sections of the dechirper. The scheme of the dechirper is the third combination type in Fig. 11: the first section is vertical and the second one is horizontal. Based on these simulations, the tolerance for the crossing angle is very relaxed, with 1% or less emittance increase even with 10° deviation from nominal.

Optimizing Beam Optics at the Dechirper

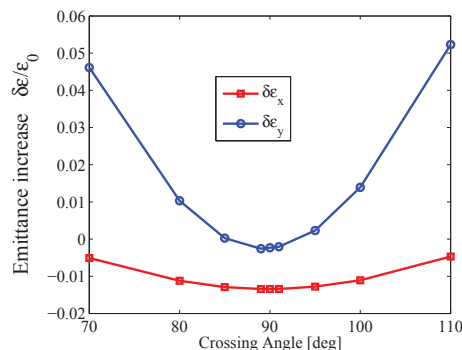From the simulations and analysis given above, we find the tolerance requirements in y are much tighter than the

ones in x. One reason for the difference is that β_y is much larger than β_x. In the simulations, we use the nominal twiss parameters of the LTU area with $\beta_y = 19m$, $\beta_x = 5m$ at the location of dechirper. If we optimize the twiss parameters for the dechirper experiment, making the β small in both planes, the tolerance introduced by the transverse wakefield can be loosened. Indeed after careful design, we can keep the β of the two planes both small (~ 7 m). In this case, the tolerance requirements for the vertical plane can be loosened by a factor ~ 2, and the experiment will be easier to carry out.

CONCLUSION

In this paper we investigated the use of a pair of flat metallic plates with small corrugations as a passive dechirper for the LCLS. We studied dechirper wakefield and fit the numerically-obtained longitudinal wake to simplified formulas, so that anyone can easily obtain the wake over a large parameter region without access to the field matching program. The fitting formulas agree well with the results of the field matching calculation. We simulated the application of the dechirper to the LCLS beam and studied the effect of the transverse wakefields. The quadrupole wakefield effect can be largely canceled out by crossing the two sections of dechirper by 90°. The dipole wakefield gives the tolerance on beam position jitter. If the expected emittance growth is to be limited to 10%, the beam position jitter should be controlled to within 20μm. In the tolerance study, the x-rotation error introduces a dipole kick, but its effect can be eliminated by offsetting the beam at the entrance of dechirper. Constraints on the error in the crossing angle are found to be quite relaxed. Smaller β values yield looser tolerances. After optimizing the twiss parameters of the LTU area, mechanical stability and positioning requirements are found to be acceptable for the current beam parameters and available diagnostics.

REFERENCES

[1] P. Emma *et al.*, PRL 112, 034801.

[2] M. Harrison *et al.*, "Removal of Residual Chirp in Compressed Beams Using a Passive Wakefield Technique" in *Proc. North American Particle Accelerator Conf.*, Pasadena, CA, USA, 2013, pp. 291-293.

[3] K. Bane and G. Stupakov, Nucl. Inst. Meth. A 690, 106 (2012).

[4] K. Bane and G. Stupakov, SLAC-PUB-15852 (2013) and LCLS-II TN-13-01.

[5] K. Bane *et al.*, SLAC-PUB-15853 (2013) and LCLS-II TN 13-02.

[6] M. Ruelas *et al.*, "Mechanical Design for a Corrugated Plate Dechirper System for LCLS", in *These Proceedings: Proc. 36th Int. Free-Electron Laser Conf.*, Basel, Switzerland, 2014, THP033.

[7] K. Bane and G. Stupakov, Phys. Rev. ST Accel. Beams 6, 023301 (2003).

[8] G. Stupakov and K. Bane, Phys. Rev. ST Accel. Beams 15, 124401 (2012).

[9] Z. Zhang *et al.*, report in preparation.

[10] R. Ischebek *et al.*, "Instrumentation and Results at the Swiss-FEL Injector Test Facility", in *Proc. 2nd Int. Beam Instrumentation Conf.*, Oxford, UK, 2013, pp. 12-18.

[11] M. Borland, ELEGANT, Advanced Photon Source LS-287, 2000.

[12] C. Behrens *et al.*, Nature Comm. 5, 3762 (2014).